Progress In Electromagnetics Research M, Vol. 50, 11–22, 2016

Magnetic Coenergy Based Modelling of PMSM for HEV/EV Application

Zaimin Zhong, Shang Jiang*, Yingkun Zhou, and Shuihua Zhou

Abstract—Permanent-magnet synchronous motors (PMSM) used for HEV/EV drive train have many nonlinear characteristics including saturation, slotting effects and non-sinusoidal back-emf. However, accurate torque control and rigorous on-board-diagnose require precise modelling that goes far beyond capacity of conventional Space Vector based PMSM model considering only fundamental frequency. By considering the higher harmonics of PMSM, this paper introduces a novel PMSM model named Generalized Space Vector Model (GSVM) based on Fourier series reconstruction of magnetic coenergy. Firstly, two-dimensional Fourier series supplemented by polynomial fitting is introduced to reconstruct the numerical solution of coenergy from Finite Element Analysis (FEA). Secondly, analytical models of flux linkage, electric torque and voltage equation in stator current oriented synchronous frame are derived based on the reconstructed coenergy model. Finally, the steady and dynamic characteristics of GSVM are validated against experimental results.

1. INTRODUCTION

PMSM are increasingly applied on HEV/EV due to the advantages including high power density, wide speed range and high efficiency [1, 2]. However, the automotive application has more rigorous demand on motor performance and on-board-diagnose. An accurate model of PMSM is the premise to solve those problems.

One type of modelling methods is based on lumped parameters — inductances L_d and L_q, which are usually regarded as constant. However, because of the saturation, slotting effects and other nonlinear factors, such a model cannot accurately describe the relationship among voltages, currents and torque. Some studies describe the saturated PMSM model by inductance variations. Both magnetic circuit and FEA analysis are applied to predict the effect of iron core saturation [3]. The inductances are illustrated by a nonlinear function respect to I_d and I_q [4–7]. However, the lumped parameter method cannot describe the space distributed property of magnetic field when the air gap flux density is not sinusoidal.

Another type of modelling methods is based on reconstructing the FEA results. The field reconstruction method (FRM) can provide a precise description of the magnetic field components for PMSM in non-sinusoidal condition, which has been applied to flux estimation and minimize torque ripple without core saturation [8–10]. A kind of flux linkage reconstruction method is put forward to predict torque ripple in saturated situation [11], but the relationship between voltages and currents is not studied. The coenergy reconstruction method is also applied to develop the PMSM model [12, 13], but the integrated representation of reconstructed coenergy is not obtained, and there is no sufficient validation of the proposed model.

This paper starts from the reconstruction of magnetic coenergy (MCE), in which all nonlinear factors are taken into account. Then a new PMSM model named GSVM, including analytical description

Received 15 June 2016, Accepted 26 August 2016, Scheduled 12 September 2016
* Corresponding author: Shang Jiang (js199199@126.com).
The authors are with the School of Automotive Studies, Tongji University, 4800 Cao'an Road, Shanghai, China.

of flux linkage, electromagnetic torque and voltage are built based on the reconstructed MCE. This form of GSVM is well organized and convenient to analyze the property of PMSM with arbitrary current or voltage excitation. The simulation results of GSVM show good accordance with the FEA and experimental results.

2. MODELLING MCE FROM NUMERICAL SOLUTIONS

2.1. Significance of MCE

The slot structure, core saturation, leakage flux and other nonlinear characteristics of PMSM can be clearly reflected by the variation in MCE. In addition, the flux linkage and electromagnetic torque can be derived from the MCE:

$$\psi_X = \frac{\partial W_c\left(i_a, i_b, i_c, \theta_r\right)}{\partial i_X} \tag{1}$$

$$T_e = \frac{3}{2} p \frac{\partial W_c\left(i_a, i_b, i_c, \theta_r\right)}{\partial \theta_r} \tag{2}$$

where W_c denotes the MCE of the PMSM, i_X the phase current, ψ_X the flux linkage of X phase, θ_r the electrical angle of rotor, p the number of pole-pairs, and T_e the electromagnetic torque.

Therefore, by describing the MCE of PMSM precisely in all working range, the full feature of PMSM can be obtained, which includes flux linkage, torque ripple, etc.

2.2. Numerical Solutions of MCE

The FEA model used in this paper is shown in Fig. 1 while its corresponding parameters are illustrated in Table 1.

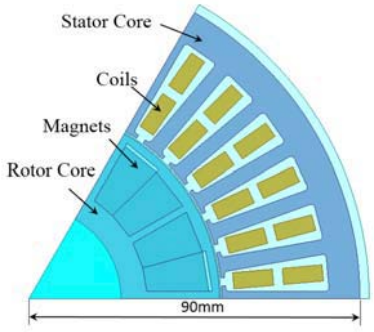

Figure 1. 2D FEA model of PMSM.

In some electromagnetic FEA software, the MCE can be obtained directly. However, the FEA software used in this paper does not have this function. Therefore, we need to get the flux linkage from FEA firstly, then integrate the flux linkage with Equation (3) to get the MCE.

$$W_c\left(i_d, i_q, \theta_r\right) = \int_0^{i_d} \psi_d\left(i'_d, 0, \theta_r\right) di'_d + \int_0^{i_q} \psi_q\left(i_d, i'_q, \theta_r\right) di'_q \tag{3}$$

where θ_r denotes the rotor position relative to A-axis; i_d and i_q are d-axis and q-axis currents, respectively; ψ_d and ψ_q are d-axis and q-axis flux linkages, respectively (Fig. 2).

The d-axis and q-axis currents can be represented by Equation (4), so the form of MCE — $W_c(i_d, i_q, \theta_r)$ can be replaced by $W_c(I_s, \theta_r, \beta)$.

$$i_d = I_s \cos\beta, \quad i_q = \sin\beta \tag{4}$$

where I_s denotes the amplitude of stator current vector in d-q synchronous-frame and β the torque angle between stator current vector and d-axis.

Table 1. Parameters of IPMSM.

Parameters	Value
Number of pole pairs	3
Number of phase	3
Number of slots	36
Outer Diameter of stator	180 mm
Inner Diameter of stator	105 mm
Outer Diameter of rotor	103.6 mm
Inner Diameter of rotor	50 mm
DC link voltage	336 V
Maximum Power	60 kW
Rated Torque	50 Nm
Rated Speed	6000 rpm

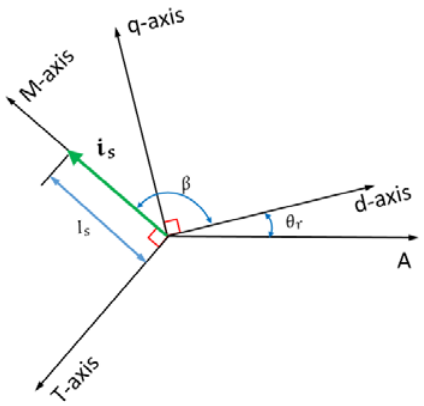

Figure 2. Synchronous-frames applied in this paper.

This paper defines that the corresponding MCE in a complete electrical period is $W_c^{k,j}(\theta_\mathbf{r})$ in working point $P^{k,j}(I_s^k, \beta^j)$, where $\theta_\mathbf{r}$ is a vector varying from 0 to 2π, comprising w_{θ_r} discrete values θ_r^i. In order to get the full MCE of PMSM, I_s^k is varied from 0 to $I_{\max}$, while β^j is varied from 0 to 2π. By combining the MCE with each given I_s, the numerical MCE with different θ_r^i and β^j can be represented by one matrix $W_c^k(\theta_\mathbf{r}, \beta)$.

2.3. Reconstruction of MCE Using Two-Dimensional Fourier Series

Many papers [14–16] have proved that the flux linkage in d-q frame consists of harmonics with 6, 12, 18, 24 ... components when excited with three-phase symmetry currents.

$$\psi_{d/q}(I_s, \theta_r, \beta) = \sum_{k=-N}^{N} C_k(I_s, \beta)\, e^{6k\theta_r}$$

So similarly the MCE deduced from Equation (3) only have harmonics with orders of $6k$ in the θ_r dimension. In addition, it is obvious that with each given I_s the excitation currents will have periodicity in the β dimension, which make the MCE also change with β with a period of 2π. Fig. 3 is the waveform of MCE from FEA numerical solution with a constant I_s and different θ_r, β, from which the periodicity of MCE in both θ_r and β dimensions can be easily observed.

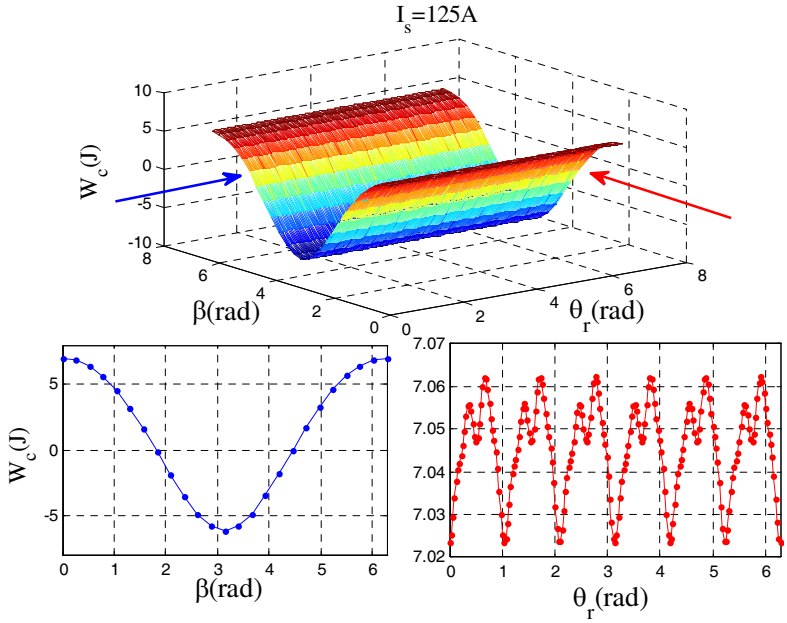

Figure 3. Periodicity of MCE in both θ_r and β dimensions.

Therefore, two-dimensional Fourier series decomposition can be employed to the discrete numerical values of MCE $W_c^k(\theta_\mathbf{r}, \beta)$ because of its periodicity. Note that for a PMSM system, the energy is concentrated around the fundamental pole frequency of the machine, thereby the number of Fourier coefficients can be reduced to a small count. Then the ultimately transformation is

$$\hat{W}_c^k(\theta_r, \beta) = \sum_{m_1=-N_1}^{N_1} \sum_{m_2=-N_2}^{N_2} C_{m_1,m_2}^k e^{jm_1\omega_\theta\theta_r + jm_2\omega_\beta\beta} \tag{5}$$

where N_1 and N_2 denote the highest Fourier series orders of θ_r and β, respectively, and C_{m_1,m_2}^k the Fourier coefficients with corresponding orders m_1 and m_2. ω_θ and ω_β are the base frequency of the MCE. With the analysis before, the value of the frequency can be easily obtained.

$$\omega_\theta = 6, \quad \omega_\beta = 1$$

2.4. Polynomial Fitting of Fourier Coefficients with Respect to Current Amplitude

When the amplitude of stator current vector I_s is fixed, the relationship among MCE W_c^k, electrical angle of rotor θ_r and torque angle β can be described by Equation (5). However, the variation trend of W_c^k with respect to I_s cannot be represented. In fact, when I_s gets larger, the core saturation may increase fast, which can change the property of PMSM and distribution of MCE largely. Thus, the next step is to construct a function to illustrate the MCE in different working points including the highly saturated region. The method used in this paper is to express the Fourier coefficients C_{m_1,m_2} of different current excitations by functions respect to $I_s - C_{m_1,m_2}(I_s)$.

In this work the polynomial fitting has been selected, then the Fourier coefficients can be represented by

$$C_{m_1,m_2}(I_s) = I_s \cdot (C_{m_1,m_2}^{N_3} I_s^{N_3} + C_{m_1,m_2}^{N_3-1} I_s^{N_3-1} + \ldots C_{m_1,m_2}^k I_s^k + \ldots + C_{m_1,m_2}^1 I_s^1 + C_{m_1,m_2}^0) \tag{6}$$

where N_3 denotes the highest order of polynomial and C_{m_1,m_2}^k the polynomial coefficient of the kth order.

Then the MCE with different I_s becomes

$$W_c(I_s, \theta_r, \beta) = \sum_{m_1=-N_1}^{N_1} \sum_{m_2=-N_2}^{N_2} C_{m_1,m_2}(I_s)\, e^{jm_1\omega_\theta\theta_r + jm_2\omega_\beta\beta}$$

Combine all the $C_{m_1,m_2}(I_s)$ into one matrix $\mathbf{C}(I_s)$ whose dimension is $2m_1+1$ by $2m_2+1$. Equation (6) becomes

$$\mathbf{C}(I_s) = I_s\left(\mathbf{C}^{N_3}I_S^{N_3} + \mathbf{C}^{N_3-1}I_S^{N_3-1} + \ldots + \mathbf{C}^{k}I_S^{k}\ldots + \mathbf{C}^{1}I_S^{1} + \mathbf{C}^{0}\right) \tag{7}$$

Introduce vectors to express the base of Fourier series

$$\begin{aligned}\mathbf{V}(\theta_r)_{1\times(2N_1+1)} &= [e^{-jN_1\omega_\theta\theta_r}, e^{-j(N_1-1)\omega_\theta\theta_r}, \ldots, e^{jk\omega_\theta\theta_r}, \ldots, e^{j(N_1-1)\omega_\theta\theta_r}, e^{jN_1\omega_\theta\theta_r}, \ldots, \\ &\quad e^{j(N_1-1)\omega_\theta\theta_r}, e^{jN_1\omega_\theta\theta_r}] \qquad (8)\\ \mathbf{U}(\beta)_{(2N_2+1)\times1} &= [e^{-jN_2\omega_\beta\beta}, e^{-jN_2-1\omega_\beta\beta}, \ldots, e^{jk\omega_\beta\beta}, \ldots, e^{j(N_2-1)\omega_\beta\beta}, e^{jN_2\omega_\beta\beta}]^T \qquad (9)\end{aligned}$$

Then the MCE is illustrated with a well organized form

$$W_C(I_S,\theta_r,\beta) = \mathbf{V}(\theta_r)\mathbf{C}(I_S)\mathbf{U}(\beta) \tag{10}$$

$\mathbf{C}^k$ are called "Distributed Matrices" in this paper. They represent the property of PMSM and are used for describing the change rules of MCE. By choosing appropriate dimension and number of matrices $\mathbf{C}^k$, the balance between accuracy and complexity of MCE model can be very flexible.

A calculation example is given by setting the orders of Fourier series and polynomial both to six, then the "Distributed Matrices" $\mathbf{C}^k$ become square matrices, with the dimension 13 by 13, and the number of "Distributed Matrices" is also 6. As shown in Fig. 4, the MCE of numerical value (marks) and analytical model (solid lines) varies with the electrical angle θ_r in almost the same track, which means that the MCE model can describe the MCE of PMSM in all working range.

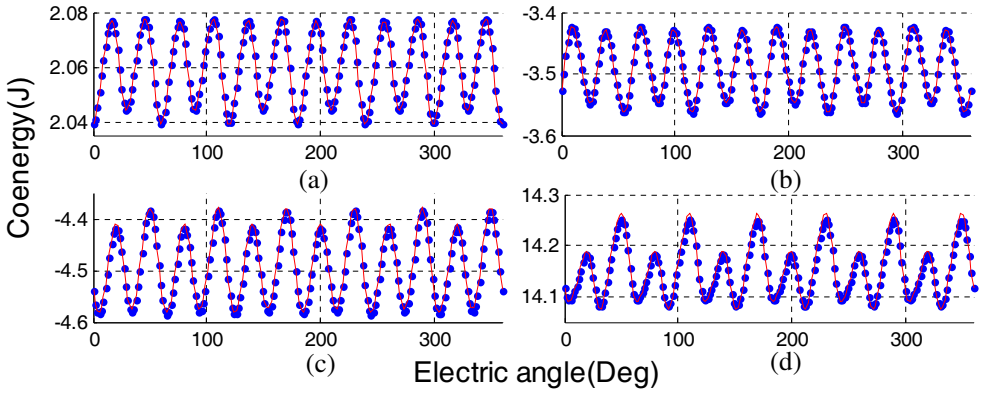

Figure 4. Variations of MCE respect to electrical angle by the numerical value (marks) and the analytical model (solid line): (a) I_s= 50A, $\beta = 45°$, (b) I_s= 125A, $\beta = 135°$, (c) I_s= 200A, $\beta = 225°$, (d) I_s= 275A, $\beta = 315°$.

There may be some doubts about the accuracy of the proposed MCE model when the excitation currents are non-sinusoidal because the model is derived from the FEA results in sinusoidal condition. However, it is clear that the MCE is only decided by its arguments — I_s, θ_r and β, thus, the model's validity is guaranteed as long as the value of MCE is accurate on every argument. Therefore, the analytical model can also express the MCE precisely even the excitation currents are non-sinusoidal.

3. PMSM MODEL DERIVED FROM MCE

3.1. Analytical Model of Flux Linkage

Equation (1) is the relationship between MCE and flux linkage in the stationary frame. In the d-q synchronous frame, the flux linkage of d-axis and q-axis will be a little more complicated.

$$\psi_d = \frac{\partial W_c(I_s,\theta_r,\beta)}{\partial i_d} = \frac{\partial W_c(I_s,\theta_r,\beta)}{\partial I_s}\cdot\frac{\partial I_s}{\partial i_d} + \frac{\partial W_c(I_s,\theta_r,\beta)}{\partial \theta_r}\cdot\frac{\partial \theta_r}{\partial i_d} + \frac{\partial W_c(I_s,\theta_r,\beta)}{\partial \beta}\cdot\frac{\partial \beta}{\partial i_d} \tag{11}$$

According to Equation (4),

$$\frac{\partial I_s}{\partial i_d} = \frac{\partial \sqrt{i_d^2+i_q^2}}{\partial i_d} = \cos\beta, \quad \frac{\partial \theta_r}{\partial i_d} = 0, \quad \frac{\partial \beta}{\partial i_d} = \frac{\partial \tan^{-1}(i_q/i_d)}{\partial i_d} = -\frac{\sin\beta}{I_s} \tag{12}$$

Substitute Equation (12) into Equation (11),

$$\psi_d = \cos\beta \cdot \mathbf{V}(\theta_r) \frac{d\mathbf{C}(I_s)}{dI_s}\mathbf{U}(\beta) - \frac{\sin\beta}{I_s} \cdot \mathbf{V}(\theta_r)\mathbf{C}(I_s)\frac{d\mathbf{U}(\beta)}{d\beta}$$

Similarly, the flux linkage of q-axis is given,

$$\psi_q = \sin\beta \cdot \mathbf{V}(\theta_r) \frac{d\mathbf{C}(I_s)}{dI_s}\mathbf{U}(\beta) + \frac{\cos\beta}{I_s} \cdot \mathbf{V}(\theta_r)\mathbf{C}(I_s)\frac{d\mathbf{U}(\beta)}{d\beta}$$

Although there is I_s in the denominator position, the form of $\mathbf{C}(I_s)$, with a sole I_s part, shown in Equation (7) makes it still have the ability to express the flux linkage when I_s is close to zero. With defining $\mathbf{D}(I_s) = \frac{\mathbf{C}(I_s)}{I_s}$, the expression of flux linkage becomes

$$\begin{bmatrix} \psi_d \\ \psi_q \end{bmatrix} = \begin{bmatrix} \cos\beta & -sin\beta \\ \sin\beta & \cos\beta \end{bmatrix} \begin{bmatrix} \mathbf{V}(\theta_r)\frac{d\mathbf{C}(I_s)}{dI_s}\mathbf{U}(\beta) \\ \mathbf{V}(\theta_r)\mathbf{D}(I_s)\frac{d\mathbf{U}(\beta)}{d\beta} \end{bmatrix} \tag{13}$$

Figure 5 shows the comparison of d-axis and q-axis flux linkages between analytical model (solid line) and FEA (marks). Plots (a) represent the d-axis and q-axis flux linkages without current excitation. The good agreement between FEA and flux linkage model has demonstrated the effectiveness of analytical model when I_s is small. Plots (b) are the flux linkage with medium current excitation, which also show a perfect consistency between two results. But when the amplitude of current excitation reaches the maximum, the deviation between the two results increases, as represented in plots (c). The reason is that the polynomial fitting cannot ensure the accuracy of derivative respect to I_s near the boundary.

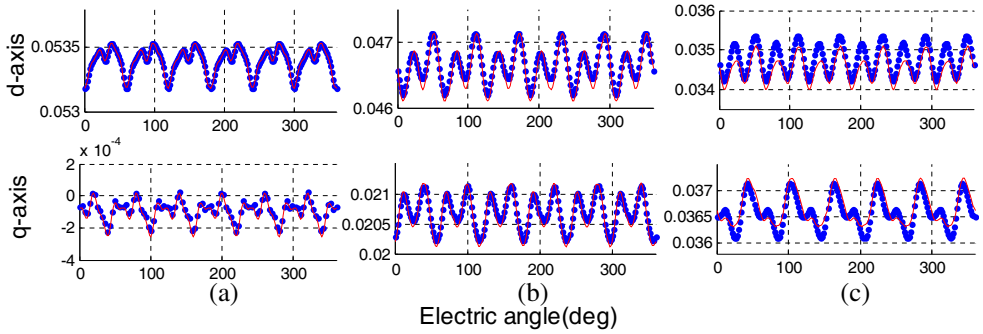

Figure 5. Variations of d-axis flux linkage (up) and q-axis flux linkage (down) respect to electrical angle by the FEA (marks) and the analytical model (solid line): (a) $I_s = 0A$, (b) $I_s = 125A$, $\beta = 135^\circ$, (c) $I_s = 300A$, $\beta = 135^\circ$.

Figure 6 illustrates d-axis and q-axis flux linkages when the injected currents are non-sinusoidal with expression (14), but the two results still match well. Thereby, the flux linage model can also represent the flux linkage precisely even if the excitation currents are non-sinusoidal. The results of flux linkage have demonstrated indirectly that the analytical model of MCE is accurate with non-sinusoidal current excitation.

$$i_a = 100\left(\cos(\theta_r+\beta) + \frac{1}{3}\cos(3\theta_r+\beta) + \frac{1}{5}\cos(5\theta_r+\beta)\right) \tag{14}$$

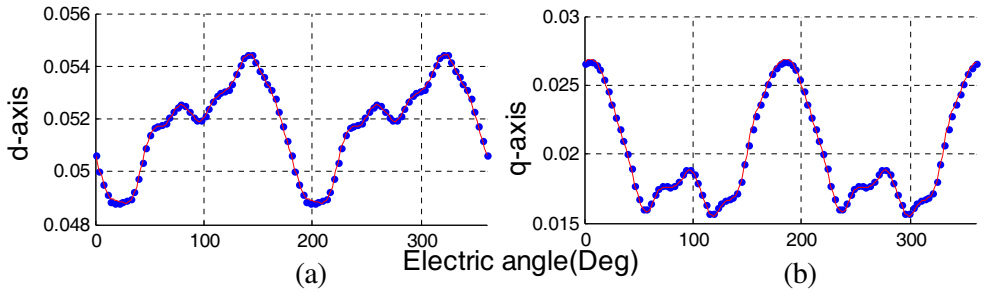

Figure 6. Variations of d-axis flux linkage (a) and q-axis flux linkage (b) respect to electrical angle by the FEA (marks) and the analytical model (solid line) with non-sinusoidal current excitation.

3.2. Analytical Model of Electro-Magnetic Torque

Just as the analytical model of flux linkage, the model of electromagnetic torque also needs to be generated in d-q synchronous-frame again.

$$T_e = \frac{3}{2}p\frac{\partial W_c\left(I_s,\theta_r,\beta\right)}{\partial\theta_r} = \frac{3}{2}p\left(\frac{\partial W_c\left(I_s,\theta_r,\beta\right)}{\partial I_s}\cdot\frac{\partial I_s}{\partial\theta_r}+\frac{\partial W_c\left(I_s,\theta_r,\beta\right)}{\partial\theta_r}\cdot\frac{\partial\theta_r}{\partial\theta_r}+\frac{\partial W_c\left(I_s,\theta_r,\beta\right)}{\partial\beta}\cdot\frac{\partial\beta}{\partial\theta_r}\right) \tag{15}$$

where $\frac{\partial I_s}{\partial\theta_r}$ can be expressed by

$$\frac{\partial I_s}{\partial\theta_r}=\frac{\partial I_s}{\partial i_d}\cdot\frac{\partial i_d}{\partial\theta_r}+\frac{\partial I_s}{\partial i_q}\cdot\frac{\partial i_q}{\partial\theta_r}$$

Then take partial derivative of i_d, i_q with respect to θ_r

$$\frac{\partial i_d}{\partial\theta_r} = i_q, \quad \frac{\partial i_q}{\partial\theta_r} = -i_d \tag{16}$$

According to Equations (4) and (16),

$$\frac{\partial I_s}{\partial\theta_r} = \frac{\partial\sqrt{i_d^2+i_q^2}}{\partial\theta_r}= 0, \quad \partial\theta_r/\partial\theta_r = 1, \quad \frac{\partial\beta}{\partial\theta_r} = \frac{\partial\tan^{-1}\left(i_q/i_d\right)}{\partial\theta_r}= -1, \tag{17}$$

Substitute Equation (17) into Equation (15),

$$T_e = \frac{3}{2}p\left(\frac{d\mathbf{V}\left(\theta_r\right)}{d\theta_r}\mathbf{C}\left(I_s\right)\mathbf{U}\left(\beta\right)-\mathbf{V}\left(\theta_r\right)\mathbf{C}\left(I_s\right)\frac{d\mathbf{U}\left(\beta\right)}{d\beta}\right) \tag{18}$$

Note that the MCE, which generates the cogging torque is not included in Equation (18), which makes the cogging torque unable to be calculated directly. Fortunately, the cogging torque changes only slightly with different current excitations, so the full torque of PMSM can be obtained by adding one constant item named $T_{cog}(\theta_r)$.

The form of torque model is very convenient to describe the change rule of torque in PMSM. Firstly, from Equation (7) we have known that the polynomial $\mathbf{C}(I_s)$ can represent the Fourier coefficients accurately even if the PMSM in a highly saturated working condition. Based on the premise, the torque model must have the ability to express the torque change on account of the core saturation. The torque comparison between FEA (marks) and torque model (solid lines) is shown in Fig. 7. It is obvious that the results of torque model are more precise than the flux linkage model compared with the FEA. The two torque results are almost the same in each electric angle regardless of the amplitude of excitation currents. The reason is that there is no derivative respect to I_s existing on the torque expression (Equation (18)). And unlike polynomial fitting respect to I_s, the two-dimensional Fourier series decomposition can guarantee not only the value, but also the derivative of MCE in each point.

Secondly, when I_s and β are constant, which means that PMSM is in its steady state with three symmetrically sinusoidal currents excitation, vector $\mathbf{V}(\theta_r)$ can separate each harmonics of torque

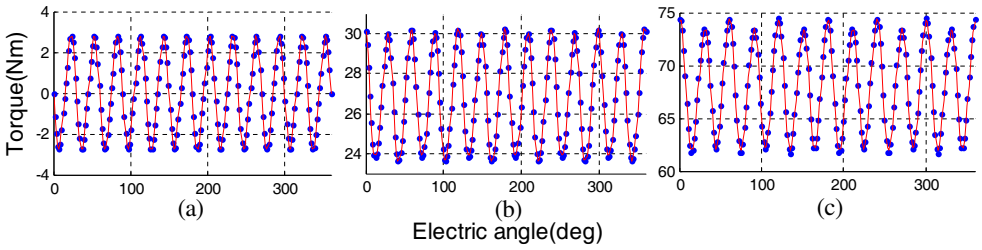

Figure 7. Variations of electric torque respect to electrical angle by the FEA (marks) and the analytical model (solid line): (a) I_s= 0A, (b) I_s= 125A, $\beta = 135°$, (c) $I_s = 300A$, $\beta = 135°$.

effectively indicated in Formula (19).

$$T_e = \begin{bmatrix} T_{-N_1} e^{-jN_1\omega_\theta\theta_r} \\ \cdots \\ T_k e^{jk\omega_\theta\theta_r} \\ \cdots \\ T_0 e^0 \\ \cdots \\ T_{N_1} e^{jN_1\omega_\theta\theta_r} \end{bmatrix} \tag{19}$$

where T_k represents the amplitude of kth torque harmonic.

Actually average torque is always used during PMSM control process. From the analytical model of torque, we find that the orders of those torque harmonics are multiple of 6, causing no average torque in each electrical period. Thus, the average torque is exactly the amplitude of zero order harmonic T_0. The formula of average torque can be simple.

$$T_0 = -\frac{3}{2} p \mathbf{V}_0(\theta_r)\, \mathbf{C}(I_s)\, \frac{d\mathbf{U}(\beta)}{d\beta}$$

where,

$$\mathbf{V}_0(\theta_r) = [0, \ldots, 0, 1, 0, \ldots 0]$$

Finally, when I_s and β vary with time severely, the excitation currents will contain a large number of harmonics. Like MCE model and flux linkage model, the torque ripple caused by non-sinusoidal current excitation can also be represented accurately by the torque model (Fig. 8).

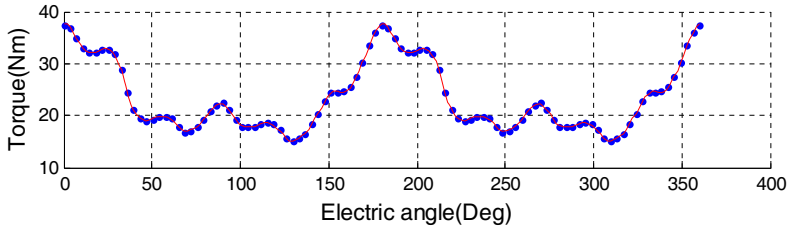

Figure 8. Variations of electric torque respect to electrical angle by the FEA (marks) and the analytical model (solid line) with non-sinusoidal current excitation.

3.3. Voltage Equations in M-T Synchronous-Frame

The flux linkage shown in Equation (13) is production of two parts. It is interesting to find that the first part is identical to the IPark transformation. Actually the second part just illustrates the flux linkage in another synchronous-frame rotated from d-q frame.

In order to express this phenomenon clearly, this paper introduces stator current oriented synchronous-frame called M-T synchronous-frame. As shown in Fig. 2, the direction of M-axis is

always aligned to the stator current vector, so the angle between M-axis and d-axis is the torque angle β. The T-axis lags the M-axis 90 degrees in space all the time.

Thus flux linkage in M-T axis is just the second part of Equation (13).

$$\begin{bmatrix} \psi_M \\ \psi_T \end{bmatrix} = \begin{bmatrix} \mathbf{V}(\theta_r)\dfrac{d\mathbf{C}(I_s)}{dI_s}\mathbf{U}(\beta) \\ \mathbf{V}(\theta_r)\mathbf{D}(I_s)\dfrac{\mathbf{dU}(\beta)}{\mathbf{d}\beta} \end{bmatrix} \tag{20}$$

It is obvious that the flux linkages in M-T frame are simpler than the results in d-q frame. Thus, this paper tries to establish the voltage equation in the M-T synchronous-frame. The components of stator current vector in M-T axis are

$$i_M = I_s, \quad i_T = 0 \tag{21}$$

Through the vector transformation $e^{j(\theta_r+\beta)}$, the vector equation in M-T axis becomes

$$\mathbf{u}_s^{MT} = R_s\mathbf{i}_s^{MT} + \frac{d\boldsymbol{\psi}_s^{MT}}{dt} + j(\omega_r+\dot{\beta})\boldsymbol{\psi}_s^{MT} \tag{22}$$

where R_s denotes the reluctance of stator windings,

$$\mathbf{u}_s^{MT} = u_M + ju_T, \quad \boldsymbol{\psi}_s^{MT} = \psi_M + j\psi_T, \quad \mathbf{i}_s^{MT} = i_M + ji_T \tag{23}$$

We find that the deviation of $\mathbf{V}(\theta_r)$ and $\mathbf{U}(\beta)$ can be expressed by multiplying one diagonal matrix algebraically.

$$\frac{d\mathbf{V}(\theta_r)}{d\theta_r} = \mathbf{V}(\theta_r)\cdot\mathbf{P}, \quad \frac{d\mathbf{U}(\beta)}{d\beta} = \mathbf{M}\cdot\mathbf{U}(\beta) \tag{24}$$

where

$$\mathbf{P} = \begin{bmatrix} -jN_1\omega_\theta & \cdots & 0 \\ \vdots & \ddots & \vdots \\ 0 & \cdots & jN_1\omega_\theta \end{bmatrix}, \quad \mathbf{M} = \begin{bmatrix} -jN_2\omega_\beta & \cdots & 0 \\ \vdots & \ddots & \vdots \\ 0 & \cdots & jN_2\omega_\beta \end{bmatrix}$$

Substituting Equations (20), (21), (23) and (24) into Equation (22), the voltage equations in M-T axis are obtained.

$$\begin{bmatrix} u_M \\ u_T \end{bmatrix} = \begin{bmatrix} R_s \\ 0 \end{bmatrix}\cdot I_s + \mathbf{A}\cdot\begin{bmatrix} \dot{I}_s \\ \dot{\beta} \end{bmatrix} + \mathbf{B}\cdot\omega_r \tag{25}$$

where

$$\mathbf{A} = \begin{bmatrix} \mathbf{V}(\theta_r) & 0 \\ 0 & \mathbf{V}(\theta_r) \end{bmatrix}\begin{bmatrix} \dfrac{d^2\mathbf{C}(I_s)}{dI_s^2} & \left(\dfrac{d\mathbf{C}(I_s)}{dI_s} - \mathbf{D}(I_s)\right)\cdot\mathbf{M} \\ \dfrac{d\mathbf{D}(I_s)}{dI_s}\cdot\mathbf{M} & \mathbf{D}(I_s)\cdot\mathbf{M}^2 + \dfrac{d\mathbf{C}(I_s)}{dI_s} \end{bmatrix}\begin{bmatrix} \mathbf{U}(\beta) & 0 \\ 0 & \mathbf{U}(\beta) \end{bmatrix}$$

$$\mathbf{B} = \begin{bmatrix} \mathbf{V}(\theta_r) & 0 \\ 0 & \mathbf{V}(\theta_r) \end{bmatrix}\begin{bmatrix} \mathbf{P}\cdot\dfrac{d\mathbf{C}(I_s)}{dI_s} - \mathbf{D}(I_s)\cdot\mathbf{M} \\ \dfrac{d\mathbf{C}(I_s)}{dI_s} + \mathbf{P}\cdot\mathbf{D}(I_s)\cdot\mathbf{M} \end{bmatrix}\begin{bmatrix} \mathbf{U}(\beta) & 0 \\ 0 & \mathbf{U}(\beta) \end{bmatrix}$$

Through this section, a new PMSM model based on the reconstructed MCE is established, including the flux linkage model, electromagnetic model and voltage model. Compared with the conventional Space Vector model based on inductances considering only fundamental frequency, this new PMSM model takes account of all the harmonic effects. Thereby, this analytic model will be called GSVM (Generalized Space Vector Model) in this paper.

Since the parameters of GSVM are only composed of several matrices, the numerical solution of GSVM is much faster than the FEA. When the orders of Fourier series and polynomial are chosen as the previous calculation example defined in Section 2.4, the computation speed of GSVM established in an off-line simulation software is about 7000 times as much as FEM. The computation time of the analytical torque model has been recorded in one main stream embedded MCU running at 160 MHz, and it only takes less than 70 microseconds. Therefore, it is possible that the GSVM can be used for model-based accurate torque control or on-board-diagnose for HEV/EV application.

4. EXPERIMENTAL VALIDATION

A test bench with a high precision torque transducer is shown in Fig. 9. The parameters of test motor in the test bench are the same as the FEA model. As flux linkages are hard to be measured accurately through the sensor devices, elements compared in this paper will be the response of electric torque and currents.

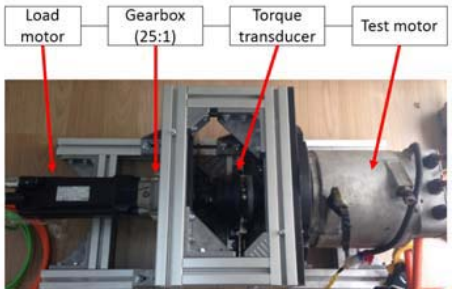

Figure 9. Test bench.

Based on the voltage Equation (25) and electric torque model (18) proposed above, the model of GSVM is established in an off-line simulation software. The close loop control system of PMSM is developed based on Field Oriental Control (FOC). And the control systems are entirely identical between the simulation and experiment. By comparing the results of GSVM and experiments in the same working condition, the accuracy of GSVM can be validated.

Firstly, the torque response in steady state is compared at different working points, as shown in Fig. 10. Plot (a) is the result of cogging torque while the remaining three plots are results with desired torque 5 Nm, 10 Nm and 15 Nm, respectively. The choices of currents distribution are based on MTPA (Maximum Torque Per Ampere) principle. It is shown that the torque responses between GSVM and experiments have good accordance, although the differences are bigger than the results comparison between GSVM and FEA. It may be caused by manufacture errors of IPMSM or the vibration of test bench.

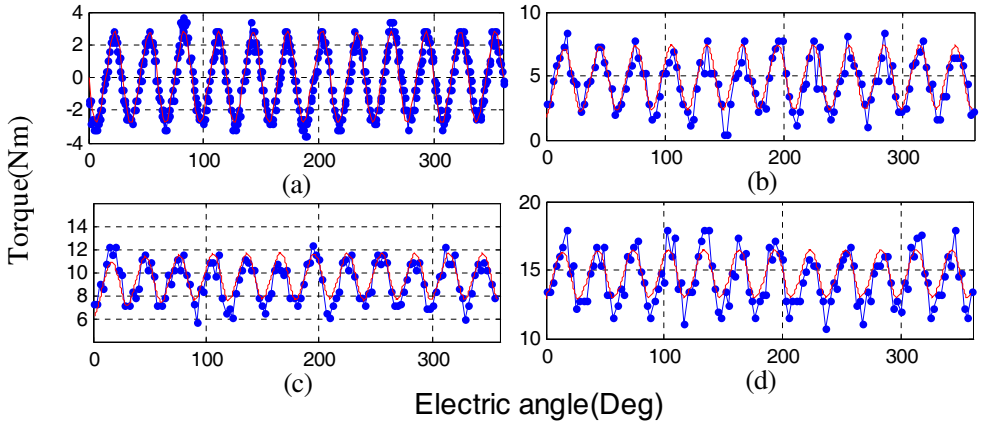

Figure 10. Variations of electric torque respect to electrical angle by experiments (marks) and GSVM (solid line): (a) I_s= 0A, (b) I_s= 20.8A, β = 103.4°, (c) I_s= 40.9A, β = 108.7°, (d) I_s= 61.4A, β = 109.7°.

Then dynamic characteristics of GSVM are tested by setting a torque step from 0 Nm to 15 Nm when the tested motor is working in a constant speed (80 rpm). In Fig. 11(a), the solid line belongs to A phase current response obtained from the simulation model GSVM while the marks come from the corresponding experimental results through one current sensor. It is obvious that the phase current

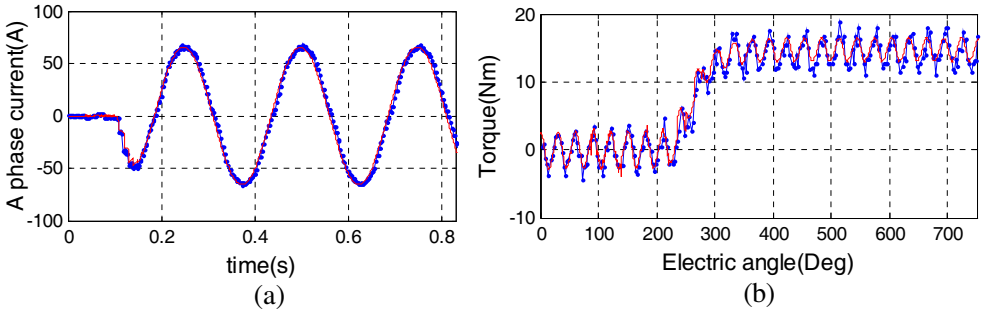

Figure 11. Comparison of dynamic response between experiments (marks) and GSVM (solid line): (a) A phase current. (b) Electric torque.

responses of two results are very close, which means that GSVM can describe the relationship between input voltages and output currents with good accuracy. The comparison of torque response between experiments (marks) and GSVM (solid line) is shown in Fig. 11(b). In fact, the response process can be divided into three parts. During the first part, the given torque is 0 Nm, but the actual torques of the two results both have fluctuation of 2.8 Nm due to slotting effects. Then the two torques increase quickly to about 15 N with almost the same trajectory. In the last part, there is a small phase difference between the two results, which is caused by speed deviation from the test bench. As a whole, the torque responses from GSVM reflect the torque property of real motor comprehensively.

5. CONCLUSIONS

This paper combines two-dimensional Fourier series and polynomial fitting to obtain an analytical model of MCE with the "Distributed Matrices" $\mathbf{C}^k$. The model of MCE has a well organized form and describes the MCE of PMSM precisely considering saturation, slotting and non-sinusoidal back-emf effects. In addition, a new PMSM model named GSVM, including the analytic description of flux linkage, electromagnetic torque and voltage is developed based on the model of MCE. The steady and dynamic characteristics have been validated by comparing with the FEA and experiment results respectively. Specifically, the GSVM can represent the flux linkage of *d*-*q*-axis and torque ripple perfectly under different current excitations. The voltage equation developed in stator current oriented synchronous frame can predict the response of three phase currents exactly.

ACKNOWLEDGMENT

This research was supported by National Natural Science Foundation of China (Grant No. 51575392).

REFERENCES

1. Cai, W., "Starting engines and powering electric loads with one machine," *IEEE Industry Applications Magazine*, Vol. 12, No. 6, 29–38, 2006
2. Zhu, Z. Q. and D. Howe, "Electrical machines and drives for electric, hybrid, and fuel cell vehicles," *Proceedings of the IEEE*, Vol. 95, No. 4, 746–765, 2007
3. Dutta, R. and M. F. Rahman, "A comparative analysis of two test methods of measuring and axes inductances of interior permanent-magnet machine," *IEEE Transactions on Magnetics*, Vol. 42, No. 12, 3712–3718, 2006.
4. Gebregergis, A., M. Islam, T. Sebastian, et al., "Evaluation of inductance in a permanent magnet synchronous motor," *2011 IEEE International Electric Machines & Drives Conference (IEMDC)*, 1171–1176, 2011.
5. Li, J. and Y. Liao, "Model of permanent magnet synchronous motor considering saturation and rotor flux harmonics," *Proceedings of the CSEE*, Vol. 31, No. 3, 60–66, 2011.

6. Stumberger, B., G. Stumberger, D. Dolina, et al., "Evaluation of saturation and cross-magnetization effects in interior permanent magnet synchronous motor," *Conference Record — IAS Annual Meeting (IEEE Industry Applications Society)*, Vol. 4, 2557–2562, 2003.
7. Wang, Y., J. Zhu, and Y. Guo, "A comprehensive analytical mathematic model for permanent-magnet synchronous machines incorporating structural and saturation saliencies," *IEEE Transactions on Magnetics*, Vol. 46, No. 12, 4081–4091, 2010.
8. Zhu, W., B. Fahimi, and S. Pekarek, "A field reconstruction method for optimal excitation of permanent magnet synchronous machines," *IEEE Transactions on Energy Conversion*, Vol. 21, No. 2, 305–313, 2006.
9. Krishnamurthy, U., "Mitigation of vibration in a permanent magnet synchronous machine using field reconstruction," *ProQuest*, 2008.
10. Khoobroo, A. and B. Fahimi, "Fault detection and optimal treatment of the permanent magnet synchronous machine using field reconstruction method," https://uta-ir.tdl.org/uta-ir/handle/10106/5115, 2010.
11. Jeong, I. and K. Nam, "Analytic expressions of torque and inductances via polynomial approximations of flux linkages," *IEEE Transactions on Magnetics*, Vol. 51, 1, 2015.
12. Stevenson, R. C., "The role of Coenergy & the development of a comprehensive analytical model for a PM motor," *IEEE Vehicle Power and Propulsion Conference, 2009, VPPC'09*, 275–282, 2009.
13. Schultz, R. D. and L. Zhao, "Coenergy based transient model of interior permanent synchronous machines," *IEEE Industry Applications Society Meeting*, 2015.
14. Xiao, X., C. Chen, and M. Zhang, "Dynamic permanent magnet flux estimation of permanent magnet synchronous machines," *IEEE Transactions on Applied Superconductivity*, Vol. 20, No. 3, 1085–1088, 2010.
15. Lu, J., J. Yang, Y. Ma, et al., "Compensation for harmonic flux and current of permanent magnet synchronous motor by harmonic voltage," *2015 International Conference on IEEE Informatics, Electronics & Vision (ICIEV)*, 1–5, 2015.
16. Liao, Y., D. Xiang, L. Ran, et al., "Analysis of harmonic transfer in an AC excited generator including speed ripple," *IEEE 2002 28th Annual Conference of the Industrial Electronics Society, IECON'02*, Vol. 2, 1162–1166, 2002.